Cationic Gold Catalysis with Pyridine-Tethered Au(III) NHC-Carbenes: An Experimental and DFT Computational Study

ARTICLE *in* ORGANOMETALLICS · JUNE 2012

Impact Factor: 4.13 · DOI: 10.1021/om3003027

5 AUTHORS, INCLUDING:

Mikko Muuronen
University of Helsinki
10 PUBLICATIONS **53** CITATIONS
SEE PROFILE

Michael Patzschke
University of Helsinki
27 PUBLICATIONS **567** CITATIONS
SEE PROFILE

ORGANOMETALLICS

Article

pubs.acs.org/Organometallics

Cationic Gold Catalysis with Pyridine-Tethered Au(III) NHC-Carbenes: An Experimental and DFT Computational Study[⊥]

Mikko Muuronen,[†,∥] Jesus E. Perea-Buceta,[†,∥] Martin Nieger,[‡,∥] Michael Patzschke,[§,∥] and Juho Helaja*[,†,∥]

[†]Laboratory of Organic Chemistry, Department of Chemistry, University of Helsinki, A. I. Virtasen aukio 1, P.O. Box 55, Helsinki, Finland

[‡]Laboratory of Inorganic Chemistry, Department of Chemistry, University of Helsinki, A. I. Virtasen aukio 1, P.O. Box 55, Helsinki, Finland

[§]Laboratory for Instruction in Swedish, Department of Chemistry, University of Helsinki, A. I. Virtasen aukio 1, P.O. Box 55, Helsinki, Finland

Supporting Information

ABSTRACT: A novel strategy is developed to produce catalytically active cationic Au(III) species by pyridine-tethered NHC complexes. The catalytic properties of two NHC complexes, equipped with distinct pyridine moieties, were studied for two catalytic benchmark reactions, the cycloisomerization of alkynylfurans to isobenzofuranoles and *o*-alkynylanilines to indoles. Optimal catalytic results were obtained employing a complex tethered with an electron-rich, *p*-methoxy-substituted pyridine. The catalysis showed high selectivity, yielding clean product conversions, while the catalytic TONs achieved in the studied reactions are well comparable with the ones reported in the literature for silver salt-activated Au(I) NHC carbene catalysts. Computational results at the DFT level support the hypothesis that equilibrating ionic complexes are the plausible catalytically active species. Computational inspection of the energetics and molecular orbital involved in the reaction reveals that the ionic state is more favored in the $AuCl_3$NHC complex equipped with the electron-rich pyridine.

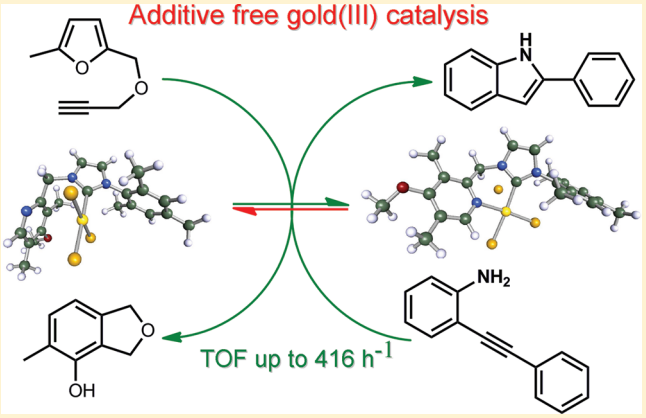

1. INTRODUCTION

Cationic Au(I) complexes bearing N-heterocyclic (NHC) carbene or phosphine ligands have recently attracted a lot of attention due to their proven excellence in various gold-catalyzed organic conversions in relation to classic "neutral" gold salts.[1,2] The superior synthetic performance of cationic gold species is noticeable in several processes, such as the activation of alkynes toward nucleophilic attack, which can proceed with excellent chemoselectivities and yields at low temperatures with rather low loadings of cationic gold catalyst, ranging typically between 0.1 and 1 mol %. In contrast, the use of neutral gold salts strictly demands a magnitude higher of loading (1−10%) and, in some cases, elevated temperatures to achieve similar conversions. But perhaps, even more important is the fact that these cationic species have been employed at the forefront of gold catalysis development in significant proof-of-concept examples of chiral counterion catalysis,[3] alkene functionalization,[4] C−H activation (sp^2 and sp^3),[2e,5] and C−C or C−X couplings involving Au(I)−Au(III) redox cycles.[6]

Technically, the cationicity can be straightforwardly implemented into NHC carbene or phosphine-coordinated gold salt ($LAuX/LAuX_3$) complexes by switching the counterion from a coordinating one, such as chloride, to a non- or weakly coordinating one. As a result, an electron-deficient coordination sphere is created around the gold nuclei. The exchange can be done by treatment of the neutral gold complex, for example, LAuCl with an external Ag(I) salt AgX (e.g., X = $^-BF_4$, ^-OTf, $^-NTf_2$), to obtain the corresponding catalytically active complex LAuX. This has proved to be a simple method that can be applied to a wide variety of gold catalysts, including such with Au(I) or Au(III) centers.[2] Recently, Nolan and co-workers reported a silver-free synthetic route to form the so-called Gagosz-type complex [Au(NTf_2)-IPr] via the "golden synthon" IPrAuOH.[7,8] The use of this weakly coordinating anion ($^-NTf_2$) has provided air-stable and isolable Au(I) phosphine and NHC complexes that do not require the usual activation with a silver-based cocatalyst.[8] To the best of our knowledge, this route has not been applied to the corresponding Au(III) analogues given that the counterion exchange is still achieved with the use of an external silver salt.

However, the use of silver salts creates some practical inconveniences due to their highly hygroscopic nature and light sensitivity, which demand some extra care to handle the

Received: April 13, 2012
Published: May 25, 2012

dx.doi.org/10.1021/om3003027 | *Organometallics* 2012, 31, 4320−4330

standard gold catalysts. Moreover, it has been shown that Au(III) can undergo reduction to Au(I) or elemental gold when an excess of silver salt is used.[9] Furthermore, the possible cocatalytic role of silver salts often introduces an uncertainty factor in any mechanistic studies,[10] also hampering the isolation of cationic gold species, consequently complicating further catalyst development studies. Industrially, highly active and persistent (TONs up to 10^5) cationic Au complexes [LAu^+X^-] with noncoordinative counterions have been prepared in harsh conditions from Au(I) methyl complexes [LAuMe] by protonating them with strong acids (e.g., HBF_4 to give BF_4^-), avoiding the use of silver salts.[11]

However, there are just a few catalytic studies in the literature on functionalized NHC Au(III) complexes.[12−14] Nevertheless, several NHC Au(III) complexes have been reported to be more stable than the corresponding Au(I) species.[13,15]

In our previous work, we prepared a zwitterionic Au(III) complex in which the gold nucleus was carrying a formal negative charge.[16] In this line, we envisioned that a similar coordination sphere of Au(III) with an NHC carbene containing a weakly coordinating ligand, such as pyridine, could produce ionic species where gold is formally positively charged. Because of geometric reasons, this strategy could be feasible for Au(III) complexes, for example, methylenepyridine-tethered NHC carbenes (Figure 1). This is moreover supported

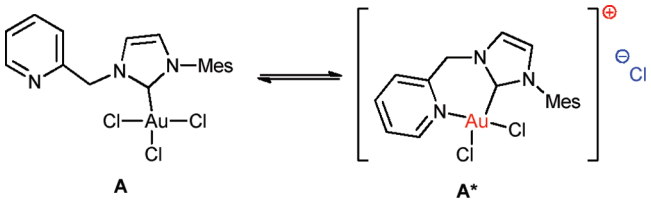

Figure 1. Equilibrium between neutral and ionic Au(III) complexes.

by recent studies on N−Au coordination.[9,14,17] In fact, complex **A** has been recently synthesized by Limbach and co-workers, but this possibility was not studied in their catalytic applications.[13] Instead, they reported the catalytic cycloisomerization of alkynylfuran to isobenzofuranol using the silver salt-activated ($AgNTf_2$) complex **A** with a moderate TON value of 112 in $CDCl_3$ at rt. On the basis of the X-ray structure of complex **A**, reported by Limbach and co-workers, we started our computational studies to gain some theoretical insight supporting our hypothesis.

Herein, we report the theoretical and experimental studies of three Au(III) complexes **A**−**C** (Scheme 1). The complexes were studied theoretically at the DFT level, and their catalytic performance was tested in benchmark reactions. Our reactions of choice were the cycloisomerization of alkynylfuran to isobenzofuranol (Scheme 2), and the intramolecular cyclization

Scheme 1. Synthesized and Studied Complexes A−C

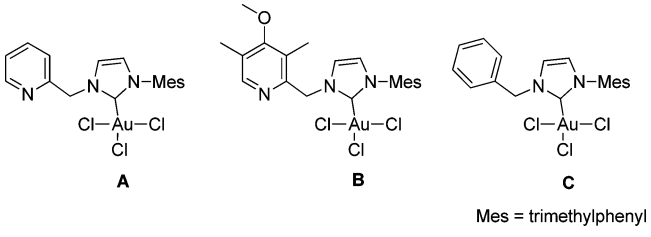

Scheme 2

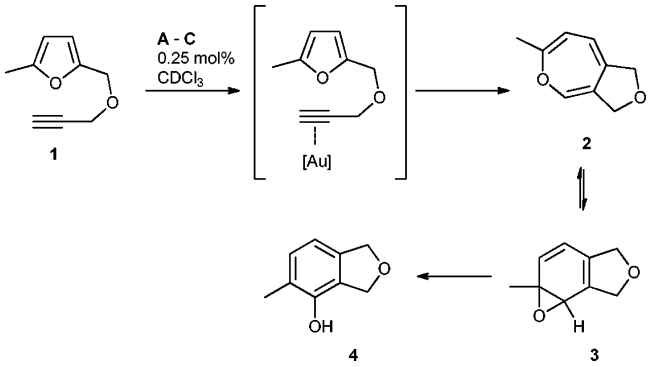

of *o*-alkylanilines to indene (Scheme 3). The former reaction has been mechanistically well-studied,[18] whereas the latter one

Scheme 3

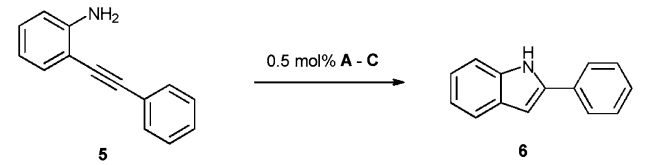

can be considered to be a straightforward intramolecular alkyne hydroamination.[19] The presented catalytic results reveal the viability of the approach, and theoretical studies combined with further discussion allow us to elucidate the origin of the activity.

2. RESULTS AND DISCUSSION

2.1. Preparation of Au(III) Complexes A−C. The imidazole salts (**LA**−**LC**) were synthesized and subsequently metalated according to the published procedures (Scheme 4).[20,13] At first, the salts were reacted with Ag_2O to generate

Scheme 4. Synthetic Route to Au(III) Complexes

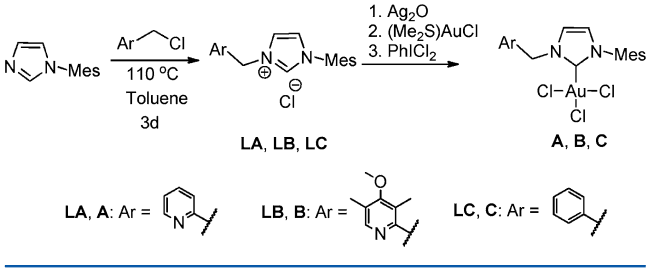

silver carbenes, and thereafter, the silver was transmetalated into Au(I) by using $(Me_2S)AuCl$ as a gold precursor, which allowed instant metathesis reaction. In turn, all the Au(I) complexes were smoothly oxidized to the corresponding Au(III) complexes **A**−**C** with $PhICl_2$ as oxidant. Pure Au(III) complexes were obtained by precipitation from dichloromethane, adding hexane, and collected by filtration. Single crystals suitable for X-ray analysis were obtained by recrystallizing the complexes in aerobic conditions from $CDCl_3$ (**A**) or dichloroethane (**B**) by a slow evaporation technique.

The literature reported X-ray structure of complex **A** was obtained from hexane.[13] Exactly the same crystal cell and structure parameters were found when we measured a single crystal formed from $CDCl_3$. The distance between the pyridine

dx.doi.org/10.1021/om3003027 | *Organometallics* 2012, 31, 4320−4330

nitrogen and the Au(III) center was 3.836 Å, indicating the lack of interaction between these two atoms in the solid phase. Additionally, X-ray analysis of complex **B**, crystallized from dichloroethane, showed a Au−N distance moderately shorter (3.418(3) Å), being still clearly outside of the coordination sphere (Figure 2).[21]

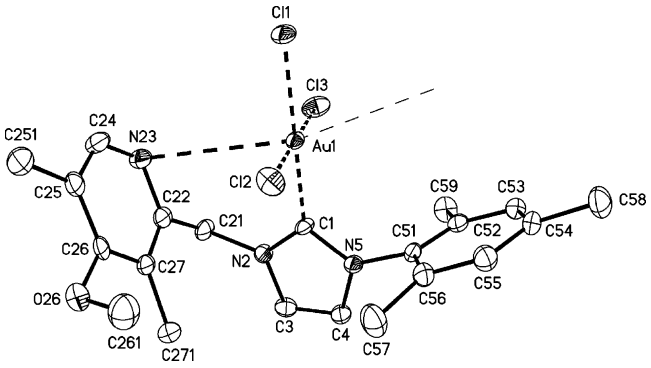

Figure 2. Molecular structure of one crystallographic complex **B**. (Displacement parameters are drawn at the 50% probability level; hydrogen atoms are omitted for clarity.) Key bond lengths (Å): Au1−N23 3.418(3), Au1−Cl1 2.316(1), Au1−Cl2 2.278(1), Au1−Cl3 2.280(1), Au1−C1 2.002(3).[21]

2.2. Catalytic Studies. Despite our unsuccessful attempts to directly coordinate the pyridine nitrogen to the gold center, as observed after X-ray analysis, we decided to test the catalytic performance in two alkyne activation reactions. We anticipated that the neutral NHC liganded Au(III) X-ray structure in Figure 2 represents the solid-state energy minimum with no available coordination sites for alkyne coordination. Additionally, the solvation and entropy increase caused by mild heating could provide a larger fraction of population of the ionic complex (Figure 1). This form might, in turn, gain the desired catalytic activity. The first test probe reaction was the cycloisomerization of alkynylfuran (**1**) to isobenzofuranol (**4**) (Scheme 2). This phenol synthesis, first reported by Hashmi,[18a] has been previously demonstrated to be a good benchmark reaction for gold catalysis.[13,22,23] The reaction mechanism is well-studied, including hypothesized and characterized intermediates **2** and **3**, respectively.

Catalytic activity was tested for all the three complexes **A**−**C** in the temperature range of 20−40 °C, except that the range was extended to 0−40 °C for complex **B** due to the observed catalytic activity (Figure 3 and Table 1). Experiments were

Table 1. Conversion of 1 to 3 and 4[a]

entry	catalyst	temp (°C)	time (h)	conversion **1** (%)[b]	yield **3** (%)[b]	yield **4** (%)[b]	TON[c]
1	**A**	20	16	9	6	3	36
2	**A**	30	16	21	5	16	84
3	**A**	40	1	16	13	0	52
		40	16	59	0	57	228
4	**B**	0	1	7	4	trace	16
		0	16	38	31	7	152
5	**B**	10	1	37	34	1	140
		10	16	67	53	11	256
6	**B**	20	1	43	39	2	164
		20	16	65	43	19	248
		20	44	65	3	59	248
7	**B**	30	1	59	52	5	228
		30	16	59	13	44	228
		30	44	59	0	57	228
8	**B**	40	1	47	38	7	180
		40	16	47	0	45	180
9	**C**	30	16	5	trace	trace	
10	**C**	40	16	7	trace	trace	

[a]Reactions were performed in $CDCl_3$ (0.2 M solution) with a catalyst loading of 0.25 mol %. [b]Determined according to the ^1H NMR integrals using 1,3,5-trimethoxybenzene as an internal standard. [c]TON = n(**1** + **3**)/n(catalyst). For a full account of the results, see the Supporting Information.

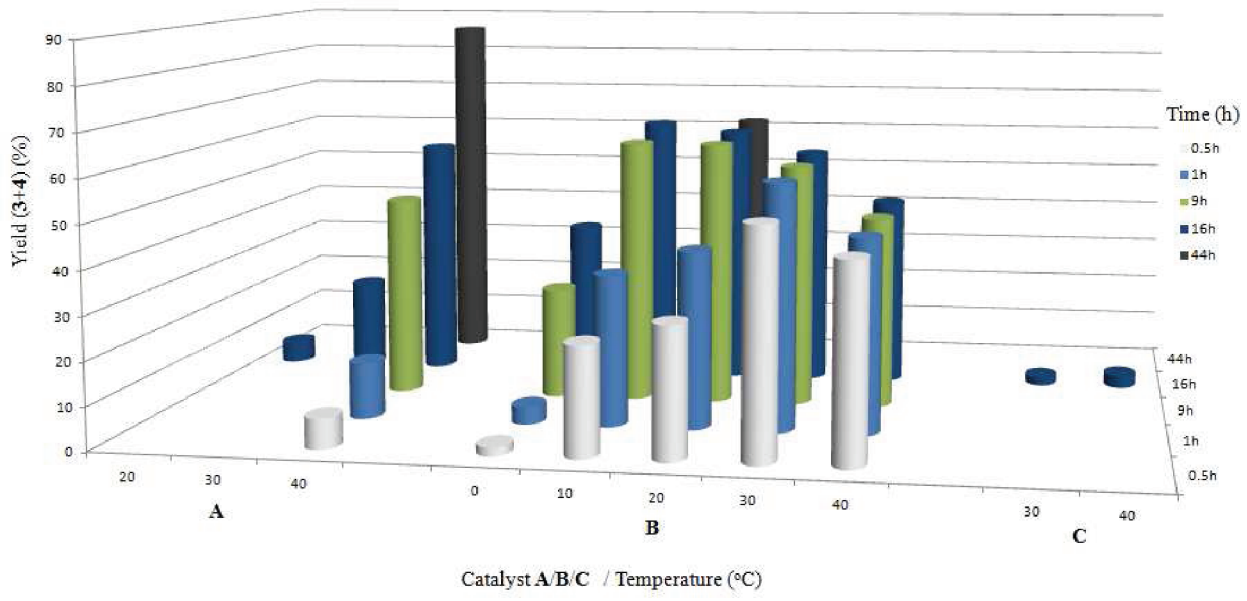

Figure 3. Conversion of **1** to **3** and **4** (yields, %) with different catalysts (**A**/**B**/**C**) at different temperatures and times. The catalytic amount used was 0.25 mol %, and the experiments were performed in $CDCl_3$ (0.2 M solution).

dx.doi.org/10.1021/om3003027 | *Organometallics* 2012, 31, 4320−4330

carried out in sealed NMR test tubes under an aerobic atmosphere. The yields were determined by relative integration of the ^{1}H NMR spectra signals using 1,3,5-trimethoxybenzene as an internal standard. While the NMR monitoring was performed below rt, we were able to identify and characterize the reaction intermediate **3** as a major, kinetic product even after 16 h of reaction time at 0−20 °C. A related intermediate has been observed and described previously by Hashmi and co-workers by subjecting slightly different substrates to analogous Au(III) catalytic conditions.[24] The ^{1}H NMR data of the intermediate are in accordance with the reported data. Moreover, the observed intermediate **3** was converted into the phenol **4** by warming up the reaction mixture. This process took place already at rt when the reaction mixture was left standing over longer periods of time (>44 h).

Our results of the catalytic experiments are displayed in Figure 3. The catalyst tests were carried out in 0.2 M $CDCl_3$ solution with 0.25 mol % catalyst loading. The most relevant experiments are displayed in Table 1. The full detailed data are included in the Supporting Information. The yields and TON values are reported by combining the intermediate **3** and product **4** yields. These numbers directly indicate the catalyst performance in activating the alkyne substrate toward nucleophilic attack.

As depicted in Figure 3, the catalytic activity was negligible for complex **C** at temperatures up to 40 °C, while only traces of product could be observed after 16 h of reaction (entries 9 and 10). This was an expectable result for an unactivated NHC gold carbene complex. Presumably, the tightly bound chlorine counterions block up the sites required on the Au nucleus for the Lewis-acidic π-alkyne coordination and concomitant activation.

Encouragingly, fairly high catalytic activation values were achieved at 40 °C for complex **A** (see Figure 3 and Table 1). The afforded yields of 57% and 85% after 16 and 44 h, respectively, with corresponding TON values of 228 and 344, respectively (entry 3), indicate undoubtedly that a plain NHC carbene tethered pyridine ring induces persistent catalytic activity for the complex. However, lowering the temperature to 30 and 20 °C slows down the catalytic activity dramatically, affording yields after 16 h of 21% (TON = 83) and 9% (TON = 35), respectively. Interestingly, the highest obtained TON value for complex **A** (344) is 3 times larger than that previously reported (112) for the same complex activated by a silver salt ($AgNTf_2$) cocatalyst.[13] However, while the reported value was obtained after 1 h of catalysis, after which the complex became inactive, the unactivated complex **A** only reached a TON value of 52 in 1 h. This gave us some room for catalyst development, as we presume that the catalytic activity of complex **A** arises from its ionic nature. Therefore, we synthesized complex **B**, in which the electron-rich pyridine moiety can be expected to possess a larger population of the ionic form.

Pleasingly, complex **B** displayed reasonable catalytic activity already at 0 °C, affording a conversion of 38% (**3**: 31%; **4**: 7%) and a TON value of 152 after 16 h of reaction time (Figure 3 and Table 1). An increase of temperature resulted in almost a 2-fold increase of the short-term turnover frequency. Indeed, a 59% conversion with a TON value of 228 was achieved already after 1 h at 30 °C. Unfortunately, the observed activity did not persist over the time; practically after an hour, the reaction did not proceed any further at this temperature. The optimal yields and TON values were accomplished at 10 °C after 16 h and 20 °C after 9 h, which were 64% (TON = 256) and 62% (TON = 248), respectively.

Figure 4 illustrates ^{1}H NMR monitoring of the kinetic performance of catalysts **A** and **B** at 40 and 10 °C, respectively.

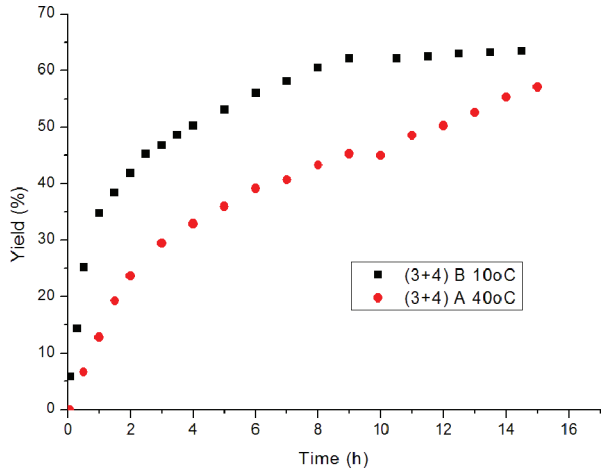

Figure 4. ^{1}H NMR monitored formation of reaction products (**3** + **4**) catalyzed by complex **B** at 10 °C (black square) and complex **A** at 40 °C (red dot).

The reaction profiles are rather similar for both catalysts. Catalyst **B** shows high activity at the start, decaying after a couple of hours. However, the reaction proceeds moderately quickly at the beginning with catalyst **A**, slowing down to some extent after a few hours, but the activity seems to still persist after 15 h.

The *o*-alkynylaniline−indole cycloisomerization reaction (Scheme 3) was selected as our second catalytic model system. It has been shown that this reaction is catalyzed in few hours by Au(III) salts, typically in protic conditions at 70−80 °C, but with rather high catalyst loadings (2−4 mol %).[19] We catalytically tested this reaction with complexes **A**−**C** in a similar manner as above. For these reactions a slightly higher catalyst loading of 0.5 mol % (0.1 M reactant solution) was used to monitor the yield evolution during 24 h (Table 2). The temperature and solvent were those parameters requiring a case-by-case tuning for optimal results.

Results presented in Table 2 reveal that the complexes **A** and **B** fail to show an efficient catalytic activity for the indole cyclization at room temperature as it was previously observed in the phenol synthesis (Table 2). However, in the case of complex **B**, raising the temperature to 50 °C afforded already a reasonable TON value of 82, while the TON of complex **A** remained still moderate (14) at this temperature. However, a raise in the temperature to 80 °C in dichloroethane improved the TON value to 44 for complex **A**. On one hand, this implies a high activation energy for this reaction, but on the other hand, it provides solid evidence for the catalyst stability at elevated temperatures. It is also worth noticing as an overall trend that the catalytic performance of all the studied complexes increased with the temperature in each solvent, reaching an optimum at 50 °C in $CHCl_3$ for complex **B**.

We also carried out catalytic control experiments for the indole cyclization by promoting cationicity into complexes **A**−**C** with a silver salt additive (AgOTf) in $CHCl_3$. As a result, a remarkable catalytic activity was observed already at room temperature. However, the selectivity drops significantly. In

dx.doi.org/10.1021/om3003027 | *Organometallics* 2012, 31, 4320−4330

Table 2. *o*-Alkynylaniline−Indole Cycloisomerization Catalysis Tests by Complexes A−C with Loadings of 0.5 mol % over 24 h Time[a]

entry	catalyst	solvent	temp (°C)	yield **6** (%)	TON
1	**A**	$CHCl_3$	20	2	4
2	**A**	$CHCl_3$	50	7	14
3	**A**	DCE	50	3	6
4	**A**	DCE	80	22	44
5	**A**	MeCN	50	4	8
6	**A**	MeCN	80	13	26
7	**B**	$CHCl_3$	20	6	12
8	**B**	$CHCl_3$	50	41	82
9	**B**	DCE	50	20	40
10	**B**	DCE	80	35	70
11	**B**	MeCN	50	6	12
12	**B**	MeCN	80	22	44
13	**C**	$CHCl_3$	20	2	4
14	**C**	$CHCl_3$	50	4	8

[a]The experiments were carried out in test tubes under a normal atmosphere.

practice, large extents of unidentified insoluble "oligomerization" products were isolated together with minor amounts of the desired cyclization products. In contrast, we observed selective, clean, indole conversions with the nonactivated complexes **A**−**C** as catalysts.

To summarize the catalytic results, it seems evident that complex **A** and especially complex **B** are able to efficiently activate alkynes without the presence of an external cocatalyst. In contrast, complex **C** does not possess any noteworthy catalytic activity at temperatures up to 50 °C. Therefore, it seems plausible that the observed catalytic activity is associated with the electron richness of the pyridine moiety, which promotes and increases the population of the ionic, catalytically active, form of the complex.

The experimental results support our initial assumption that the pyridine ring, especially the one functionalized with electron-donating groups (**B**), brings population to the ionic state already at ambient temperatures. Also, the fact that the unactivated complexes **A** and **B** catalyze selectively two different alkyne activation reactions, that is, for alkene versus amine nucleophile, implies a wider applicability for the developed concept. Finally, complex **B** was the most active catalyst for both alkyne activations, even though its activity was not persistent in the phenol synthesis.

2.3. Computational Studies. To gain theoretical insight for the observed catalytic activity, we performed computational studies for the complexes **A** and **B** at the DFT level to elucidate the differences between both their neutral states (**A**/**B**) and their ionic states (**A***/**B***). Throughout the next sections, results of these calculations, such as differences in geometries, electronic structures, and formation energies, are discussed.

All calculations were performed at the DFT level employing the TPSS functional of Tao, Perdew, Staroverov, and Scuseria.[25] Gas-phase optimized structures were optimized as well using the B3LYP functional of Becke to compare the geometries with two different methods.[26] The multipole accelerated resolution of the identity approximation, MARI-J, was used with suitable fitting basis sets.[27,28] Dispersion effects were taken in to account by Grimme's D3 dispersion correction.[29] The Triple-ζ quality basis set (def2-TZVPP) was used in all computations.[30] Vibrational frequencies were calculated to ascertain that all the optimized structures are true minima on the potential hypersurface. Scalar relativistic effects were included by using the Stuttgart ECP for gold.[31] The effect of the solvent was taken into account by the COSMO method, which was used with the ε value of chloroform (4.81).[32]

*Structures of **A** and **B**.* The key bond lengths obtained from geometry optimizations and crystal structure analysis for complexes **A** and **B** are listed in Table 3, and gas-phase

Table 3. Bond Lengths from Optimized Geometries in Å[a]

	Au−$C_{carbene}$	Au−Cl(1)	Au−Cl(2)	Au−Cl(3)	Au−N_{pyr}
A crystal[13]	1.999	2.3201	2.2906	2.2905	3.836
A	2.03	2.32	2.33	2.31	4.06
A (solv)	2.03	2.34	2.33	2.31	3.98
A (w)	2.03	2.32	2.32	2.32	4.13
A (w, solv)	2.03	2.34	2.32	2.32	4.05
A B3LYP	2.04	2.33	2.34	2.32	4.16
B crystal[21]	2.002	2.3161	2.2775	2.2799	3.418
B	2.03	2.32	2.32	2.33	3.3
B (solv)	2.03	2.34	2.33	2.32	3.29
B (w)	2.03	2.32	2.31	2.34	3.26
B (w, solv)	2.03	2.34	2.31	2.33	3.27
B B3LYP	2.04	2.33	2.33	2.33	3.3

[a]Optimizations were carried with the TPSS-D3 functional unless noted otherwise; the def2-TZVPP basis set was used in all cases. (w) indicates the usage of four explicit water molecules in the optimization. (solv) indicates the usage of the COSMO solvating model using an ε value of 4.81.

computed geometries of **A** and **B** are presented in Figure 5. In most cases, the agreement between computed and experimental parameters is sufficiently accurate with distances typically matching within 0.04 Å. However, as an exception, the predicted distances between the gold and the pyridine nitrogen differ notably from X-ray analyzed ones (0.23 Å for **A** and 0.11 Å for **B**). We ascribe these differences to packing effects in the crystal structures. Moreover, we believe that the active catalysts, solvated complexes, are better described by the computational techniques used. Both methods, TPSS and B3LYP, yielded very similar results. Including solvent effects on the complexes with the COSMO model affects mostly the distance between gold and the pyridine nitrogen.

To mimic the reaction media, a small water cluster (four molecules) was included into the computations. This was relevant, because the reactions were performed in open air and some amount of moisture is present in the solvents. It has recently been shown in the mechanistic study by Hashmi and co-workers of a gold-catalyzed reaction that an inclusion of a similar water cluster gives better correspondence between computed and experimental results.[33]

The inclusion of four water molecules did have only small effects on the bond distances in the structures of **A** and **B** (Table 3 and Figure 6). In optimized structures, the water molecules are hydrogen-bonded to each other, forming chains between the pyridine nitrogen and one of the Au-coordinated chloride atoms (Figure 6). The closest N−H distance is 1.81 Å for complex **A** and 1.77 Å for complex **B**; meanwhile, the shortest H−Cl distances are 2.43 and 2.49 Å for **A** and **B**, respectively.

*Stuctures of **A*** and **B***. The ionic structures of **A*** and **B*** were optimized by the same approach (Table 4 and Figure 7). Also, in this case, both TPSS and B3LYP methods gave similar

dx.doi.org/10.1021/om3003027 | *Organometallics* 2012, 31, 4320−4330

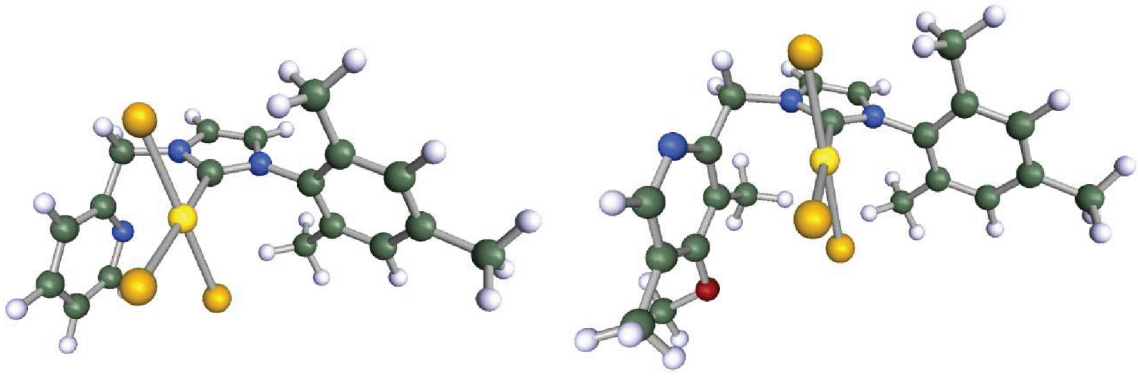

Figure 5. Optimized gas-phase geometries (TPSS-D3 def2-TZVPP) for complexes **A** and **B**.

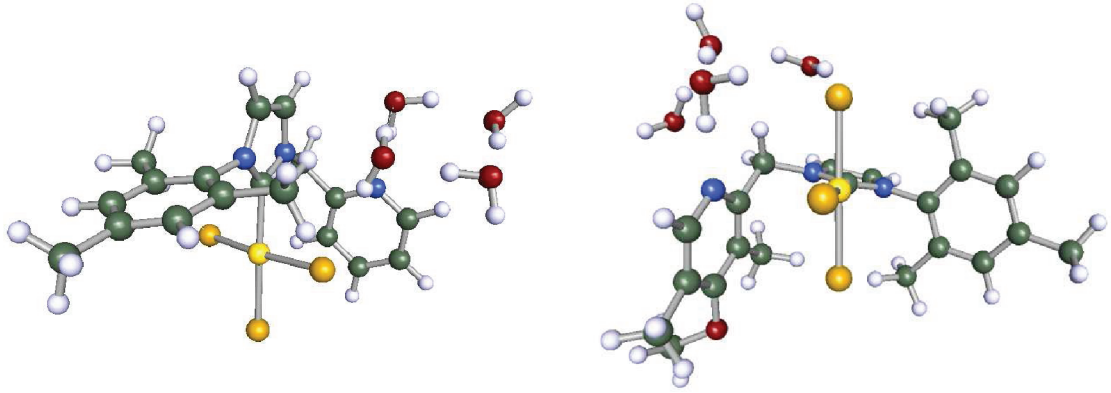

Figure 6. Optimized gas-phase geometries with four explicit water molecules (TPSS-D3 def2-TZVPP) for complexes **A** and **B**.

Table 4. Bond Lengths from Optimized Geometries in Å[a]

	Au−$C_{carbene}$	Au−Cl(1)	Au−Cl(2)	Au−Cl(3)	Au−N_{pyr}
A*	2.03	2.33	2.3	3.06	2.14
A* (solv)	2.02	2.34	2.3	3.06	2.11
A* (w)	2.02	2.35	2.29	3.29	2.11
A* (w, solv)	2.02	2.36	2.29	3.41	2.1
A* B3LYP	2.04	2.34	2.3	3.19	2.15
B*	2.03	2.34	2.3	3.09	2.13
B* (solv)	2.01	2.35	2.3	3.09	2.1
B* (w)	2.02	2.35	2.29	3.31	2.1
B* (w, solv)	2.01	2.36	2.3	3.41	2.09
B* B3LYP	2.03	2.35	2.3	3.22	2.14

[a]Optimizations were carried out with the TPSS-D3 functional unless noted otherwise; the def2-TZVPP basis set was used in all cases. (w) indicates the usage of four explicit water molecules in the optimization. (solv) indicates the usage of the COSMO solvating model using an ε value of 4.81.

results in the gas phase, except that the latter one produced 0.13 Å longer Au−Cl(3) distances. The solvation of these complexes with COSMO models did not induce any notable changes on the geometries. The inclusion of the water cluster increased the Au−Cl(3) distances by 0.23 and 0.22 Å in the complexes **A*** and **B*** in the gas phase, respectively (Table 6 and Figure 8). The combination of solvating effects and the water cluster increases the Au−Cl(3) distance further to 3.41 Å in both cases. This is well above the typical coordinative bonding distance and can be explained by the ability of water to solvate ions by hydrogen bonding. The shortest H−Cl distance with the water cluster and Cl(3) in the gas phase is 2.07 and 2.05 Å for complexes **A*** and **B***, respectively. Solvating these complexes did not affect the hydrogen-bonding distances.

NBO Charge Densities. To gain insight into the electronic structure, the NBO charges for the important atoms are presented in Table 5. Inclusion of the solvent (COSMO) did have only a minor impact on the geometries (Tables 3 and 6). However, the electronic structure should be better described when taking solvent effects into account. A pronounced effect can be expected, especially in the case of strongly polarized ionic forms, since the solvent would stabilize the partial charges in solution.

An inspection of Table 5 reveals that the atomic charges are redistributed from the nonionic states (**A**/**B**) to the corresponding ionic states (**A***/**B***), as can be expected. The removal of one chloride from gold slightly increases the cationicity of gold, whereas the detached chloride (Cl3) gains more charge. Interestingly, the negative charge of the pyridine nitrogen is increased in the ionic form to some extent. This effect is more notable in the case of complex **B**, in which the oxygen of *p*-methoxy pyridine is capable of acting as an electron donor. In both cases, the imidazole carbene stabilizes the changes on the gold nuclei, as can be observed on the change of NBO charge in the carbene carbon. The influence of the water cluster on the NBO charges was only minor, and it did not cause any additional differences between neutral and ionic states.

Overall, the differences in geometries and NBO charges between **A*** and **B*** are fairly small, being inadequate to explain the observed reactivity differences. These results indicate rather that both ionic states (**A***/**B***) are more activated than their corresponding nonionic states (**A**/**B**) and are bearing similar

dx.doi.org/10.1021/om3003027 | *Organometallics* 2012, 31, 4320−4330

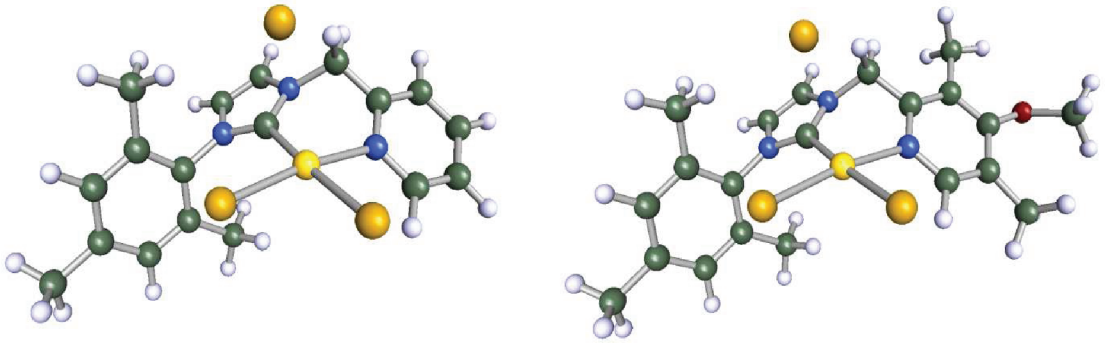

Figure 7. Optimized geometries (TPSS-D3/def2-TZVPP) for **A*** and **B*** in the gas phase.

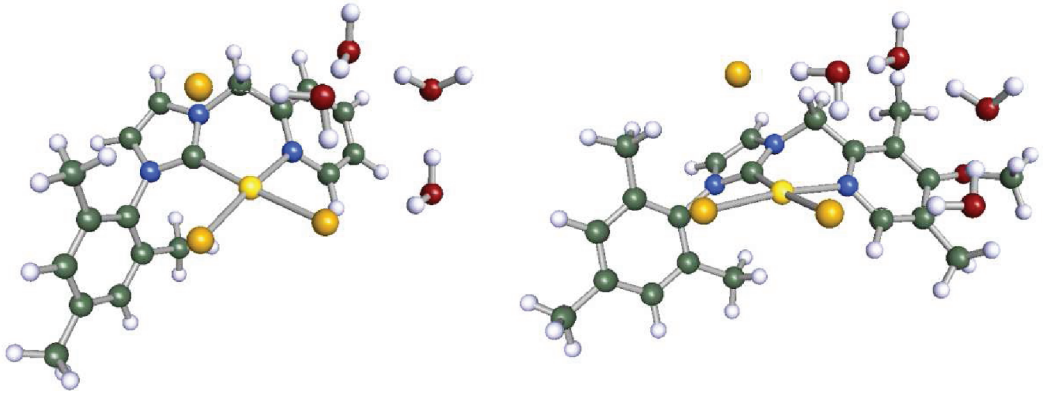

Figure 8. Optimized structures (TPSS-D3/def2-TZVPP) for **A*** and **B*** with four explicit water molecules in the gas phase.

Table 5. NBO Natural Charges Based on TPSS-D3/def2-TZVPP Optimized Structures in Solvent Phase (ε = 4.81)

	Au	N_{pyr}	$C_{carbene}$	Cl(1)	Cl(2)	Cl(3)	O
A	1.00815	−0.43088	0.21221	−0.55157	−0.45568	−0.48151	
A*	1.11742	−0.43765	0.18974	−0.5420	−0.42629	−0.86726	
B	1.0159	−0.42875	0.21322	−0.54905	−0.46303	−0.47057	−0.49152
B*	1.11764	−0.44096	0.19392	−0.54768	−0.43533	−0.87454	−0.45737

Table 6. Reaction Enthalpies (ΔH) and Gibbs Free Energies (ΔG) at 298.15 K between the Ground State and the Ionic Complex[a]

reaction	ΔE (gas)	ΔG (gas)	ΔG (solv)
1. **A** → **A***	21.3	22.5	9.9
2. **A** (w) → **A*** (w)	16.3	15.3	7.1
3. **B** → **B***	18.3	19.2	7.5
4. **B** (w) → **B*** (w)	9.4	12.4	6.7
5. **A** + (w) → **A** (w)	−15.6	−1.3	4.1
6. **A*** + (w) → **A*** (w)	−20.6	−8.4	1.3
7. **B** + (w) → **B** (w)	−16.4	5.1	1.0
8. **B*** + (w) → **B*** (w)	−25.2	−11.8	0.2

[a]Units are in kcal/mol. (w) indicates the usage of four explicit water molecules in the optimization.

characteristics in their catalytic performance. Therefore, we reasoned that the catalytic activity could be directly related to the populations of ionic forms. On these grounds, we decided to compare the formation energies of the ionic complexes.

Formation Energies. The reaction enthalpies and the Gibbs free energies for the formation of ionic species at room temperature in gas and solvent phases (298.15 K) are shown in Table 6 (reactions 1−4). Furthermore, the stabilization energies gained by adding the small water cluster are listed correspondingly (Table 6, reactions 5−8).

The gas-phase reaction enthalpies (Table 6) are too high to bring population to the ionic state, 21.3 and 18.3 kcal/mol in the reactions A → A* and B → B*, respectively. This comes as no surprise, as ions are not stabilized in the gas phase. Accordingly, the gas-phase reaction free energies display a similar trend. However, both reaction energies are notably stabilized by the water cluster, yet the values are still too high to explain the reactivity. Nevertheless, the inclusion of solvent effects brings these reaction energies down to 9.9 and 7.5 kcal/mol, while the addition of explicit water molecules decreases the energies to even more accessible values of 7.1 and 6.7 kcal/mol for **A** and **B**, respectively.

These solution-phase computed ΔG values indicate that the populations in the zwitterionic complexes would be negligible. For the reaction energy of 6 kcal/mol, the Boltzmann distribution gives a population of 0.004% in the ionic state at room temperature. However, even small errors in these energies have a significant impact on the populations; that is, the reaction energy of 3 kcal/mol would give an almost 1% population in the ionic state under the same conditions. We assume that this fraction would be already enough for the reaction to proceed. Such low populations (below 1%) are in

dx.doi.org/10.1021/om3003027 | *Organometallics* 2012, 31, 4320−4330

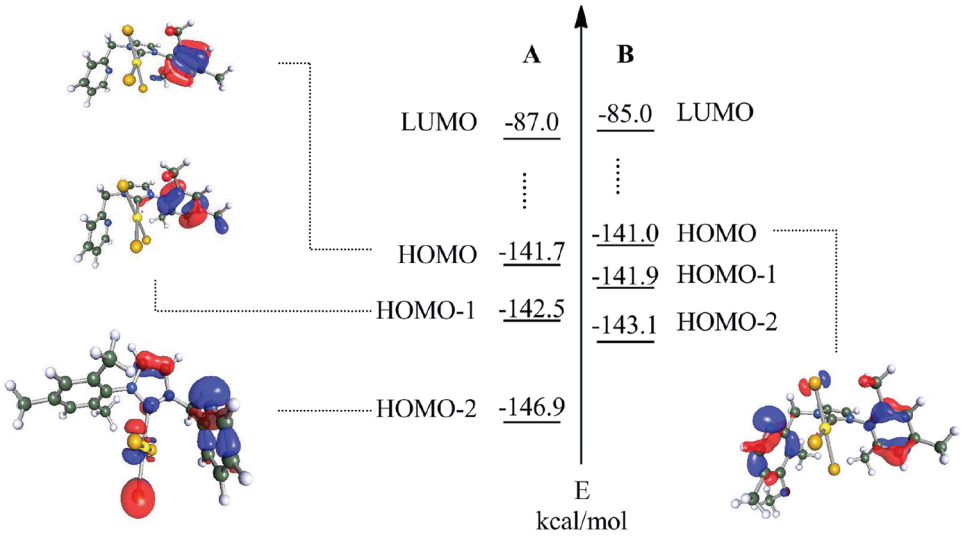

Figure 9. Orbital diagram of the first unoccupied and the three highest occupied orbitals of **A** and **B** in solution (TPSS-D3/def2-TZVPP). Units are in kcal/mol.

agreement with our ^{1}H NMR studies of **A** and **B** in the temperature range of −5 to 50 °C, in which only one (the nonionic) species was detected in $CDCl_3$ (see the Supporting Information).

To explain the reactivity differences between **A** and **B**, a more useful approach is to compare the $\Delta\Delta G$ values where substantial error cancellation can be expected. The $\Delta\Delta G$ value in solution for the formation of zwitterionic complexes between **A** and **B** shows an energy difference of 2.4 kcal/mol, favoring the ionic state of complex **B** over **A**. Inclusion of a water cluster reduces this solution-phase $\Delta\Delta G$ value to 0.4 kcal/mol. It should be noted, however, that the placement of water molecules is in no way unique. Therefore, the $\Delta\Delta G$ of 2.4 kcal/mol is less ambiguous.

The $\Delta\Delta G$ value is in good agreement with our experimental results where the temperature range of usage for complex **B** was approximately 30 °C lower than that with complex **A** (Figure 4). According to the Boltzmann distribution, such a $\Delta\Delta G$ value can give a substantial difference between the populations of ionic forms between **A** and **B**, favoring **B*** rather than **A***. Moreover, this is supported by the ESI-HRMS measurements where the molecular cation of **B*** was detected, whereas **A*** was not populated in concentrations high enough to be visible.

Molecular Orbitals. To further analyze the reactivity, we compared the molecular orbitals of complexes **A** and **B**. From Figure 1, it can be deduced that the most important orbital for the formation of **A*** and **B*** is the one containing the "lone pair" on the pyridine nitrogen. In Figure 9, we plot the highest occupied orbitals containing the pyridine nitrogen lone pair from solution-phase optimized structures for complexes **A** and **B**. In both cases, the LUMO is located on the gold−chlorine antibonding orbital. For complex **A**, we find the electron density for the pyridine nitrogen at HOMO-2, whereas the HOMO and HOMO-1 are mainly constructed with the π orbitals of trimethylphenyl. The corresponding orbital for complex **B** is already the HOMO. The energy difference between the respective orbitals for **A** and **B** is 6 kcal/mol, favoring complex **B**. The energy gap difference between the corresponding occupied orbital and LUMO shows a very similar behavior favoring complex **B** as expected. The orbital picture is quite consistent with our free reaction energy analysis and the experimental results.

Finally, a word on the accuracy of the employed methods: with our DFT approach, we should be able to reach an accuracy in reaction energies of around 4−6 kcal/mol.[34] However, our results should be even more reliable, as we are mostly looking at differences of energy differences, thereby getting a substantial systematic error cancellation.

3. CONCLUSIONS

A novel concept has been developed for additive-free cationic Au(III) catalysis based on pyridine-tethered NHC-Au(III) carbenes. The pyridine-linked side-arms activate Au(III) NHC complexes toward alkynes, as was demonstrated in the benchmark reactions. The catalytic activity of the complexes correlates well with the electron richness of the pyridine moiety. The experimental results together with theoretical computations suggest that the equilibrating ionic species, in which Au(III) has a positive charge, are the active catalysts.

The current work is a proof-of-concept study that demonstrates that instant cationicity around the gold nucleus is a valuable tool in homogeneous gold catalyst development. When all NHC complex platforms are taken in comparison for the phenol synthesis, the complexes **A** and **B** stay still an order of magnitude behind the best reported TON values.[18f] This indicates that there is still room to develop this concept further. Our primary future interest is the variation of coordinative moieties and ligand electronic properties to achieve more efficient Au(III) catalysts.

4. EXPERIMENTAL SECTION

4.1. General. In the computational part, the vibrational data were also used in the calculation of thermodynamical data, such as Gibbs energies, in the following way. The structures were optimized in the gas phase, and a frequency calculation was performed to get the chemical potential (c.p.). We then optimized the structure using the COSMO approach (ε = 4.81) and finally did a gas-phase single-point calculation of that structure. The Gibbs energy was then calculated as

$$\Delta G = E(\text{gas}) + \text{c.p.} + (E(\text{COSMO}) - E(\text{gas})@\text{COSMO}))$$

All computations were done with the Turbomole program package, version 6.31.[35] Standard parameters were employed, except for the

dx.doi.org/10.1021/om3003027 | *Organometallics* 2012, 31, 4320−4330

DFT grid. Here, we used the finer m5 grid throughout. Pictures of molecular orbitals and geometries were made with the TmoleX graphical user interface. Orbital pictures were constructed using isovalues of 0.05.

All the transmetalation reactions were performed under argon using standard Schlenk techniques. DCM was distilled over CaH_2. All the other solvents were obtained as HPLC quality and used as received. ^1H and ^{13}C NMR spectra were recorded at room temperature (except the reaction kinetics experiments) using a Varian Mercury 300 or Varian Inova 500 machine. ^1H and ^{13}C spectra were referenced to the solvent signals (in $CDCl_3$, 7.26 and 77.16 ppm, respectively; in d6-DMSO, 2.50 and 39.52 ppm, respectively). High-resolution mass spectra (EI) were obtained on MS JEOL JMS-700 and HR-ESI MS with Bruker MicroTOF instruments.

Compounds **1** and **4** were synthesized and characterized according to the literature as well as **5** and **6**.[18c,23,19c,37] Trimethylphenylimidazole and $PhICl_2$ were prepared as reported.[38,39] Me_2SAuCl was prepared by directly mixing Me_2S and $HAuCl_4$ in methanol and collected by filtration.

4.2. X-ray Data of B. Crystals suitable for X-ray diffraction of **B** were grown from dichloroethane solution. Crystal structure determinations was performed on a Nonius KappaCCD diffractometer at 123(2) K using Mo Kα radiation (λ = 0.71073 Å). Direct methods were used for structure solution (SHELXS-97),[36] refinement was carried out using SHELXL-97 (full-matrix least-squares on F^2), and hydrogen atoms were refined using a riding model. A semiempirical absorption correction was applied.

Data for **B**: yellow crystals, $C_{21}H_{25}AuClN_3O-C_2H_4Cl_4$, M_r = 737.71, crystal size = 0.08 × 0.16 × 0.24 mm, monoclinic, space group $P2_1/c$ (No. 14), a = 16.1402(16) Å, b = 9.678(1) Å, c = 17.512(1) Å, β = 97.745(5)°, V = 2710.6(3) Å^3, Z = 4, ρ = 1.808 Mg/m^{-3}, μ(Mo Kα) = 5.942 mm^{-1}, T = 123(2) K, $F(000)$ = 1440, $2\theta_{max}$ = 55°, 32 271 reflections, of which 6199 were independent (R_{int} = 0.046), 304 parameters, R_1 = 0.029 (for $I > 2\sigma(I)$), wR_2 = 0.057 (all data), S = 1.06, largest diff. peak/hole = 1.208/−0.718 e Å^{-3}.[21]

4.3. Synthesis and Characterization. *Trimethylphenylimidazole.* Yellowish solid, yield 70%. ^1H NMR ($CDCl_3$, 300 MHz): δ 7.43 (1H, t, J = 1.1 Hz), 7.23 (1H, t, J = 1.1 Hz), 6.96 (2H, d, J = 0.6 Hz), 6.88 (1H, t, J = 1.1 Hz), 2.34 (3H, s), 1.98 (6H, s). ^{13}C NMR ($CDCl_3$, 75 MHz): δ 139.0, 137.6, 134.6, 133.5, 129.7, 129.1, 120.2, 21.1, 17.4.

*4.3.1. General Procedure for the Synthesis of Imidazole Salts **A**/**B**-**L**.*[20] The hydrochloride salt of the correponding 2-chloromethyl pyridine precursor (2.8 mmol) was dissolved in toluene (5 mL) and neutralized with a K_2CO_3 saturated aqueous solution. After extraction, the organic phase was subsequently poured onto a flask with trimethyphenylimidazole (2.6 mmol). The mixture was stirred at 110 °C for 3 days. Filtration of the resulting precipate and further washing with toluene afforded the corresponding pure imidazole salt **A**/**B**-**L**.

*1-(2,4,6-Trimethylphenyl)-3-(2-pyridylmethyl)imidazolium Chloride (**A**-**L**):*[20] White solid, yield 74%, mp 231−235 °C. ^1H NMR (d6-DMSO, 300 MHz): δ 9.85 (1H, t, J = 1.7 Hz), 8.57−8.51 (1H, m), 8.15 (1H, t, J = 1.7 Hz), 7.99 (1H, t, J = 1.7 Hz), 7.91 (1H, td, J = 7.7, 1.7 Hz), 7.57 (1H, d, J = 7.7 Hz), 7.44−7.38 (1H, m), 7.15 (2H, s), 5.77 (2H, s), 2.33 (3H, s), 2.05 (6H, s). ^{13}C NMR (d6-DMSO, 75 MHz): δ 153.4, 149.5, 140.2, 138.7, 137.5, 134.3, 131.2, 129.2, 123.9, 123.7, 123.6, 122.3, 53.1, 20.6, 16.9. HRMS (EI) calculated for $C_{18}H_{19}N_3$ m/z 277.1579 (M). Found 277.1592.

*1-(2,4,6-Trimethylphenyl)-3-((4-methoxy-3,5-dimethyl-)2-pyridylmethyl)imidazolium Chloride (**B**-**L**):* White solid, yield 75%, mp 208−209 °C. ^1H NMR (d6-DMSO, 300 MHz): δ 9.62 (1H, t, J = 1.7 Hz), 8.13 (1H, s), 8.03 (1H, t, J = 1.7 Hz), 7.95 (1H, t, J = 1.7 Hz), 7.16 (2H, s), 5.73 (2H, s), 3.76 (3H, s), 2.34 (3H, s), 2.29 (3H, s), 2.21 (3H, s), 2.08 (6H, s). ^{13}C NMR (d6-DMSO, 75 MHz): δ 163.6, 151.3, 148.8, 140.2, 139.1, 134.3, 131.2, 129.2, 125.8, 124.4, 123.6, 123.3, 60.0, 51.2, 20.6, 16.8, 12.8, 10.1. HRMS (EI) calculated for $C_{21}H_{25}N_3O$ m/z 335.1998 (M). Found 335.2003.

*1-(2,4,6-Trimethylphenyl)-(2-benzyl)imidazolium Chloride (**C**-**L**):* Prepared as **A**/**B**-**L** from benzyl chloride and trimethylphenylimidazole. White solid, yield 53%, mp 216−218 °C. ^1H NMR (d6-DMSO, 300 MHz): δ 9.86 (1H, t, J = 1.7 Hz), 8.13 (1H, t, J = 1.7 Hz), 7.97 (1H, t, J = 1.7 Hz), 7.54−7.37 (5H, m), 7.15 (2H, s), 5.59 (2H, s), 3.33 (3H, s), 2.33 (3H, s), 2.01 (6H, s). ^{13}C NMR (d6-DMSO, 75 MHz): δ 140.2, 137.8, 135.0, 134.1, 131.4, 129.2, 129.0, 128.7, 128.2, 124.2, 123.2, 52.0, 20.5, 16.9. HRMS (EI) calculated for $C_{19}H_{20}N_2$ m/z 276.1626 (M). Found 276.1625.

*4.3.2. General Procedure for Au(III) Complexes **A**−**C**.* All the steps in this procedure were done using dry solvents under argon, protecting as much as possible the reaction mixtures from light. Filtration of the intermediate complexes was done under air. The corresponding imidazole salt (0.27 mmol) and Ag_2O (0.18 mmol) were stirred in DCM (7 mL) at rt for 16 h. The reaction mixture was then filtrated through a short pad of Celite to remove the unreacted Ag_2O, and the solvents were evaporated. The resulting silver complex was allowed to react with $(Me_2S)AuCl$ (0.27 mmol) in DCM (7 mL) for 24 h. Filtration of the reaction mixture through Celite, followed by evaporation in vacuo, afforded the corresponding Au(I) complex that was immediately dissolved in 17 mL of DCM. After addition via cannula at 0 °C of a DCM (10 mL) solution of $PhICl_2$ (0.32 mmol), the resulting reaction mixture was allowed to stir overnight at rt. After evaporation, the pure product was precipitated from a small amount of DCM with hexane. Product was collected by filtration and dried in vacuo.

*Trichloro[1-(2-pyridinylmethyl)-3-(2,4,6-trimethylphenyl)-2H-imidazol-2-ylidene]gold (**A**):*[13] Pale yellow solid, yield 84%, mp 183−186 °C. ^1H NMR ($CDCl_3$, 500 MHz): δ 8.66 (1H, d, J = 4.3 Hz), 7.84 (1H, td, J = 7.7, 1.3 Hz), 7.72−7.66 (2H, m), 7.38 (1H, dd, J = 7.7, 4.3 Hz), 7.10 (1H, d, J = 1.7 Hz), 6.98 (2H, s), 5.69 (2H, s), 2.34 (3H, s), 2.13 (6H, s). ^{13}C NMR ($CDCl_3$, 126 MHz): δ 152.4, 150.0, 143.8, 141.2, 138.4, 135.5, 132.4, 130.0, 125.3, 124.7, 124.6, 124.6, 56.1, 21.3, 18.6. Anal. Calcd for $C_{18}H_{19}AuCl_3N_3$: C, 37.23; H, 3.30; N, 7.24. Found: C, 37.46; H, 3.52; N, 6.81.

*Trichloro[1-((4-methoxy-3,5-dimethyl-)2-pyridylmethyl)-3-(2,4,6-trimethylphenyl)-2H-imidazol-2-ylidene]gold (**B**):* Pale yellow solid, yield 77%, mp 197−200 °C. ^1H NMR ($CDCl_3$, 500 MHz): δ 8.29 (1H, s), 7.74 (1H, s, broad), 7.09 (1H, s), 6.97 (2H, s), 5.71 (2H, s), 3.89 (3H, s), 2.53 (3H, s), 2.33 (3H, s), 2.32 (3H, s), 2.13 (6H, s). ^{13}C NMR ($CDCl_3$, 126 MHz): δ 165.8, 149.7, 149.6, 143.3, 141.1, 135.6, 132.6, 130.0, 127.7, 126.9, 125.4, 124.7, 60.6, 53.3, 21.3, 18.6, 13.7, 11.8. HRMS (ESI) calculated for $C_{21}H_{25}AuCl_2N_3O$ m/z 602.1035 $(M)^+$. Found 602.1027. Anal. Calcd for $C_{21}H_{25}AuCl_3N_3O$: C, 39.49; H, 3.94; N, 6.58. Found C, 38.64; H, 3.96; N, 6.21.

*Trichloro[1-(2-benzyl)-3-(2,4,6-trimethylphenyl)-2H-imidazol-2-ylidene]gold (**C**):* Pale yellow solid, yield 81%, mp 245−249 °C. ^1H NMR ($CDCl_3$, 500 MHz): δ 7.46 (5H, s, broad), 7.15 (1H, d, J = 1.9 Hz), 7.08 (1H, d, J = 1.9 Hz), 7.00 (2H, s), 5.61 (2H, s), 2.35 (3H, s), 2.17 (6H, s). ^{13}C NMR ($CDCl_3$, 126 MHz): δ 143.8, 141.2, 135.5, 132.8, 132.4, 130.1, 129.8, 129.8, 129.2, 125.7, 123.2, 55.4, 21.3, 18.7, HRMS (ESI) calculated for $C_{21}H_{23}AuCl_2N_3$ m/z 584.0929 (M + MeCN)$^+$. Found 584.0930. Anal. Calcd for $C_{19}H_{20}AuCl_3N_2$: C, 39.37; H, 3.48; N, 4.83. Found: C, 38.59; H, 3.47; N, 4.71.

4.4. Catalytic Studies. All conversions and yields were determined according to the relative integration of the ^1H NMR respective signals using 1,3,5-trimethoxybenzene as an internal standard. Reactions were done under an aerobic atmosphere. In phenol synthesis, the total concentration was 0.2 and 0.1 M during the indole cyclization.

4.4.1. Phenol Synthesis. A 0.40 mL portion of a base solution of **1** (0.333 mmol/mL, including internal standard 0.0446 mmol/mL) was placed in a test tube. A 0.20 mL aliquot of the catalyst base solution (**A**/**B**/**C** 1.72 μmol/mL, 0.25 mol %) was added, and the tube was sealed. The tube, including stirrer, was placed into an oil bath at the corresponding temperature. The ^1H NMR spectrum was measured directly from the reaction solution after the proposed time when $CDCl_3$ was used as solvent.

*2-(5-Methyl)furylmethyl Propargyl Ether (**1**):* ^1H NMR ($CDCl_3$, 500 MHz): δ 6.24 (1H, d, J = 3.0 Hz), 5.92 (1H, dd, J = 3.0, 1.0 Hz), 4.49 (2H, s), 4.16 (2H, d, J = 2.4 Hz), 2.45 (1H, t, J = 2.4 Hz); 2.29 (3H, d, J = 1.0 Hz). ^{13}C NMR ($CDCl_3$, 126 MHz): δ 153.1, 149.0, 111.3, 106.4, 79.6, 74.8, 63.3, 56.7, 13.7.

4-Methyl-1,3-dihydroisobenzofuran-5-ol (4): ^{1}H NMR ($CDCl_3$, 500 MHz): δ 7.04 (1H, d, J = 7.5 Hz), 6.71 (1H, d, J = 7.5 Hz), 5.13 (2H, s), 5.10 (2H, s), 2.25 (3H, s). ^{13}C NMR ($CDCl_3$, 126 MHz): δ 148.5, 139.2, 130.6, 125.3, 122.0, 112.9, 74.1, 71.8, 15.2.

1a-Methyl-1a,4,6,6b-tetrahydrooxireno[2,3-e]isobenzofuran (3): ^{1}H NMR ($CDCl_3$, 500 MHz): δ 6.23 (1H, d, J = 9.3 Hz), 6.19 (1H, d, J = 9.3 Hz), 4.90 (2H, t, J = 4.5 Hz), 4.77 (2H, t, J = 4.5 Hz), 4.01 (1H, s), 1.68 (3H, s).

4.4.2. Indole Cyclization. A 0.050 mmol portion of **5** was placed in a test tube with 0.35 mL of solvent, followed by 0.15 mL of the catalyst base solution (1.72 μmol/mL, 0.50 mol %). The test tube was then sealed and stirred in an oil bath at the desired temperature. Solvents were evaporated, and the internal standard was added. The ^{1}H NMR samples were prepared directly from the mixture.

2-(Phenylethynyl)aniline (5):[19c] ^{1}H NMR (500 MHz, $CDCl_3$): δ 4.28 (2H, s), 6.69−6.77 (2H, m), 7.15 (1H, td, J = 7.7, 1.5 Hz), 7.31−7.41 (4H, m), 7.50−7.57 (2H, m). ^{13}C NMR (126 MHz, $CDCl_3$): δ 147.9, 132.3, 131.6, 129.9, 128.5, 128.3, 123.4, 118.1, 114.5, 108.1, 94.8, 86.0.

2-Phenyl-1H-indole (6):[37] ^{1}H NMR (500 MHz, $CDCl_3$): δ 6.85 (1H, m), 7.14 (1H, td, J = 7.0, 0.9 Hz), 7.21 (1H, td, J = 7.0, 1.1 Hz), 7.33 (1H, m), 7.40 (1H, dd, J = 8.1, 0.7 Hz), 7.42−7.47 (2H, m), 7.62−7.70 (3H, m), 8.45 (1H, s). ^{13}C NMR (126 MHz, $CDCl_3$): δ 138.0, 137.0, 132.5, 129.4, 129.1, 127.8, 125.3, 122.4, 120.8, 120.4, 111.0, 100.1.

■ ASSOCIATED CONTENT

Supporting Information

Complete table of phenol synthesis catalytic results, optimized Cartesian coordinates and energies for the presented systems, ^{1}H and ^{13}C NMR spectra of complexes **A**, **B**, and **C**. This material is available free of charge via the Internet at http://pubs.acs.org.

■ AUTHOR INFORMATION

Corresponding Author

*E-mail: juho.helaja@helsinki.fi.

Author Contributions

[‖]The manuscript was written through contributions of all authors. All authors have given approval to the final version of the manuscript.

Funding

[⊥]This work was partially supported by the Academy of Finland [J.H., No. 118586 and 113317].

Notes

The authors declare no competing financial interest.

■ ACKNOWLEDGMENTS

M.Sc. Tom Wirtanen and Dr. Petri Heinonen are accredited for the HRMS measurements. The National Centre for Scientific Computing (CSC) is acknowledged for computational resources. Dr. Uwe Huniar from COSMOlogic GmbH and Dr. Nino Runeberg from CSC are greatly acknowledged for technical support with the Turbomole program.

■ REFERENCES

(1) Au(I) NHC reviews: (a) Nolan, S. P. *Acc. Chem. Res.* **2011**, *44*, 91−100. (b) Gaillard, S.; Cazin, C. S. J.; Nolan, S. P. *Acc. Chem. Res.* DOI: 10.1021/ar200188f. Selected NHC-Au(I) complex preparations: (c) Hashmi, A. S. K.; Lothschütz, C.; Böhling, C.; Hengst, T.; Hubbert, C.; Rominger, F. *Adv. Synth. Catal.* **2010**, *352*, 3001−3012. (d) Hashmi, A. S. K.; Lothschütz, C.; Graf, K.; Häffner, T.; Schuster, A.; Rominger, F. *Adv. Synth. Catal.* **2011**, *354*, 1407−1412. (e) Hashmi, A. S. K.; Riedel, D.; Rudolph, M.; Rominger, F.; Oeser, T. *Chem.—Eur. J.* **2012**, *18*, 3827−3830.

(2) Selected Au catalysis reviews: (a) Fürstner, A.; Davies, P. W. *Angew. Chem., Int. Ed.* **2007**, *46*, 3410−3449. (b) Hashmi, A. S. K. *Chem. Rev.* **2007**, *107*, 3180−3211. (c) Hashmi, A. S. K.; Hutchings, G. *Angew. Chem., Int. Ed.* **2006**, *45*, 7896−7936. (d) C−X bond-forming reactions: Corma, A.; Leyva-Perez, A.; Sabater, M. J. *Chem. Rev.* **2011**, *111*, 1657−1712. (e) C−H functionalizations: Boorman, T. C.; Larrosa, I. *Chem. Soc. Rev.* **2011**, *40*, 1910−1925. (f) Heterocycles from Au catalysis: Rudolph, M.; Hashmi, A. S. K. *Chem. Commun.* **2011**, *47*, 6536−6544. (g) Addition to C−C multiple bonds: Huang, H.; Zhou, Y.; Liu, H. *Beilstein J. Org. Chem.* **2011**, *7*, 897−936.

(3) (a) Hamilton, G. L.; Kang, E. J.; Mba, M.; Toste, F. D. *Science* **2007**, *317*, 496−499. (b) Ito, Y.; Sawamura, M.; Hayashi, T. *J. Am. Chem. Soc.* **1986**, *108*, 6405−6406. (c) Pastor, S. D.; Togni, A. *Helv. Chim. Acta* **1991**, *74*, 905−933. (d) Hashmi, A. S. K *Nature* **2007**, *449*, 292−293.

(4) (a) Brenzovich, W. E., Jr.; Benitez, D.; Lackner, A. D.; Shunatona, H. P.; Tkatchouk, E.; Goddard, W. A., III; Toste, F. D. *Angew. Chem., Int. Ed.* **2010**, *49*, 5519−5522. (b) Melhado, A. D.; Brenzovich, W. E., Jr.; Lackner, A. D.; Toste, F. D. *J. Am. Chem. Soc.* **2010**, *132*, 8885−8887. (c) de Haro, T.; Nevado, C. *Angew. Chem., Int. Ed.* **2011**, *50*, 906−910.

(5) (a) de Haro, T.; Nevado, C. *Synthesis* **2011**, *16*, 2530−2539. (b) Hashmi, A. S. K.; Schäfer, S.; Wölfle, M.; Diez Gil, C.; Fischer, P.; Laguna, A.; Blanco, M. C.; Gimeno, M. C. *Angew. Chem., Int. Ed.* **2007**, *46*, 6184−6187.

(6) (a) Zhang, G.; Peng, Y.; Cui, L.; Zhang, L. *Angew. Chem., Int. Ed.* **2009**, *48*, 3112−3115. (b) de Haro, T.; Nevado, C. *Chem. Commun.* **2011**, *47*, 248−249. (c) Hashmi, A. S. K.; Ramamurthi, T. D.; Rominger, F. *J. Organomet. Chem.* **2009**, *694*, 592−597.

(7) (a) Gaillard, S.; Slawin, A. M. Z.; Nolan, S. P. *Chem. Commun.* **2010**, *46*, 2742−2744. (b) Gaillard, S.; Bosson, J.; Ramon, R. S.; Nun, P.; Slawin, A. M. Z.; Nolan, S. P. *Chem.—Eur. J.* **2010**, *16*, 13729−13740.

(8) (a) Ricard, L.; Gagosz, F. *Organometallics* **2007**, *26*, 4704−4707. (b) Mezailles, N.; Ricard, L.; Gagosz, F. *Org. Lett.* **2005**, *7*, 4133−4136.

(9) Topf, C.; Hirtenlehner, C.; Fleck, M.; List, M.; Monkowius, U. *Z. Anorg. Allg. Chem.* **2011**, *637*, 2129−2134.

(10) Patrick, S. R.; Boogaerts, I. I. F.; Gaillard, S.; Slawin, A. M. Z.; Nolan, S. P. *Beilstein J. Org. Chem.* **2011**, *7*, 892−896.

(11) Teles, J. H.; Brode, S.; Chabanas, M. *Angew. Chem., Int. Ed.* **1998**, *37*, 1415−1418.

(12) Boronat, M.; Corma, A.; González-Arellano, C.; Iglesias, M.; Sánchez, F. *Organometallics* **2010**, *29*, 134−141.

(13) Pazický, M.; Loos, A.; Ferreira, M. J.; Serra, D.; Vinokurov, N.; Rominger, F.; Jäkel, C.; Hashmi, A. S. K.; Limbach, M. *Organometallics* **2010**, *29*, 4448−4458.

(14) Mendivil-Tomás, E.; Toullec, P. Y.; Díez, J.; Conejero, S.; Michelet, V.; Cadierno, V. *Org. Lett.* **2012**, *14*, 2520−2523.

(15) Topf, C.; Hirtenlehner, C.; Zabel, M.; List, M.; Fleck, M.; Monkowius, U. *Organometallics* **2011**, *30*, 2755−2764.

(16) Melchionna, M.; Nieger, M.; Helaja, J. *Chem.—Eur. J.* **2010**, *16*, 8262−8267.

(17) (a) Kriechbaum, M.; List, M.; Berger, R. J. F.; Patzschke, M.; Monkowius, U. *Chem.—Eur. J.* **2012**, *18*, 5506−5509. (b) Khin, C.; Hashmi, A. S. K.; Rominger, F. *Eur. J. Inorg. Chem.* **2010**, 1063−1069.

(18) (a) Hashmi, A. S. K.; Frost, T. M.; Bats, J. W. *J. Am. Chem. Soc.* **2000**, *122*, 11553−11554. (b) Hashmi, A. S. K.; Weyrauch, J. P.; Rudolph, M.; Kurpejovic, E. *Angew. Chem., Int. Ed.* **2004**, *43*, 6545−6547. (c) Hashmi, A. S. K.; Wölfle, M.; Ata, F.; Hamzic, M.; Salathé, R.; Frey, W. *Adv. Synth. Catal.* **2006**, *348*, 2501−2508. (d) Hashmi, A. S. K.; Rudolph, M.; Bats, J. W.; Frey, W.; Rominger, F.; Oeser, T. *Chem.—Eur. J.* **2008**, *14*, 6672−6678. (e) Rudolph, M.; McCreery, M. Q.; Frey, W.; Hashmi, A. S. K. *Beilstein J. Org. Chem.* **2011**, *7*, 794−801. (f) Hashmi, A. S. K.; Yu, Y.; Rominger, F. *Organometallics* **2012**, *31*, 895−904.

(19) (a) Arcadi, A.; Bianchi, G.; Marinelli, F. *Synthesis* **2004**, 610−618. (b) Majumdar, K. C.; Samanta, S.; Chattopadhyay, B. *Tetrahedron Lett.* **2008**, *49*, 7213−7216. (c) Brand, J. P.; Chevalley, C.; Waser, J. *Beilstein J. Org. Chem.* **2011**, *7*, 565−569. (d) Hashmi, A. S. K.;

Ramamurthi, T. D.; Rominger, F. *Adv. Synth. Catal.* **2010**, *352*, 971−975.
(20) Cisnetti, F.; Lemoine, P.; El-Ghozzi, M.; Avignant, D.; Gautier, A. *Tetrahedron Lett.* **2010**, *51*, 5226−5229.
(21) Crystallographic data (excluding structure factors) for the structures reported in this work have been deposited with the Cambridge Crystallographic Data Centre as supplementary publication no. CCDC-875527 (complex **B**). Copies of the data can be obtained free of charge on application to The Director, CCDC, 12 Union Road, Cambridge DB2 1EZ, U.K. (Fax: int. code +(1223)336-033. E-mail: deposit@ccdc.cam.ac.uk).
(22) Hashmi, A. S. K.; Wölfle, M.; Ata, F.; Hamzic, M.; Salathé, R.; Freya, W. *Adv. Synth. Catal.* **2006**, *348*, 2501−2508.
(23) Chen, Y.; Yan, W.; Akhmedov, N. G.; Shi, X. *Org. Lett.* **2010**, *12*, 344−347.
(24) Hashmi, A. S. K.; Rudolph, M.; Weyrauch, J. P.; Wölfle, M.; Frey, W.; Bats, J. W. *Angew. Chem., Int. Ed.* **2005**, *44*, 2798−2801.
(25) Tao, J.; Perdew, J. P.; Staroverov, V. N.; Scuseria, G. E. *Phys. Rev. Lett.* **2003**, *91*, 146401.
(26) (a) Becke, A. D. J. *Chem. Phys.* **1993**, *98*, 5648. (b) Lee, C.; Yang, W.; Parr, R. G. *Phys. Rev. B* **1988**, *37*, 785−789.
(27) Sierka, M.; Hogekamp, A.; Ahlrichs, R. *J. Chem. Phys.* **2003**, *118*, 9136−9148.
(28) (a) Eichkorn, K.; Weigend, F.; Treutler, O.; Ahlrichs, R. *Theor. Chem. Acc.* **1997**, *97*, 119−124. (b) Weigend, F. *Phys. Chem. Chem. Phys.* **2006**, *8*, 1057−1065. (c) Hellweg, A.; Hättig, C.; Höfener, S.; Klopper, W. *Theor. Chem. Acc.* **2007**, *117*, 587−597.
(29) Grimme, S.; Antony, J.; Ehrlich, S.; Krieg, H. *J. Chem. Phys.* **2010**, *132*, 154104.
(30) (a) Schäfer, A.; Huber, C.; Ahlrichs, R. *J. Chem. Phys.* **1994**, *100*, 5829−5835. (b) Weigend, F.; Häser, M.; Patzelt, H.; Ahlrichs, R. *Chem. Phys. Lett.* **1998**, *294*, 143−152. (c) Weigend, F.; Ahlrichs, R. *Phys. Chem. Chem. Phys.* **2005**, *7*, 3297−3305.
(31) Andrae, D.; Haeussermann, U.; Dolg, M.; Stoll, H.; Preuss, H. *Theor. Chim. Acta* **1990**, *77*, 123.
(32) Schäfer, A.; Klamt, A.; Sattel, D.; Lohrenz, J. C. W.; Eckert, F. *Phys. Chem. Chem. Phys.* **2000**, *2*, 2187−2193.
(33) (a) Krauter, C. M.; Hashmi, A. S. K.; Pernpointner, M. *ChemCatChem* **2010**, *2*, 1226−1230. (b) Hashmi, A. S. K.; Pernpointner, M.; Hansmann, M. M. *Faraday Discuss.* **2011**, *152*, 179−184.
(34) Goerigk, L.; Grimme, S. *Phys. Chem. Chem. Phys.* **2011**, *13*, 6670−6688.
(35) (a) Ahlrichs, R.; Baer, M.; Haeser, M.; Horn, H.; Koelmel, C. *Chem. Phys. Lett.* **1989**, *162*, 165−169. (b) Treutler, O.; Ahlrichs, R. *J. Chem. Phys.* **1995**, *102*, 346−354. (c) Von Arnim, M.; Ahlrichs, R. *J. Comput. Chem.* **1998**, *19*, 1746−1757. (d) Von Arnim, M.; Ahlrichs, R. *J. Chem. Phys.* **1999**, *111*, 9183−9190.
(36) Sheldrick, G. M. *Acta Crystallogr., Sect. A* **2008**, *64*, 112−122.
(37) Koradin, C.; Dohle, W.; Rodriguez, A. L.; Schmid, B.; Knochel, P. *Tetrahedron* **2003**, *59*, 1571−1581.
(38) Liu, J.; Chen, J.; Zhao, J.; Li, L.; Zhang, H. *Synthesis* **2003**, *17*, 2661−2666.
(39) Zhao, X.-F.; Zhang, C. *Synthesis* **2007**, *4*, 551−557.